DEVELOPMENT AND VALIDATION OF HIGH-PRECISION CFD METHOD WITH VOLUME-TRACKING ALGORITHM FOR GAS-LIQUID TWO-PHASE FLOW SIMULATION ON UNSTRUCTURED MESH

I1. Kei Ito [1, 2], I2. Tomoaki Kunugi [1], I3. Hiroyuki Ohshima[2]

[1] Department of Nuclear Engineering, Kyoto University,
Yoshida, Sakyo-ku, Kyoto-shi, Kyoto,606-8501, Japan
Tel:+81-29-267-4141, Fax:+81-29-266-3675, E-mail:ito.kei@jaea.go.jp
[2] Advanced Nuclear System Research and Development Directorate, Japan Atomic Energy Agency

Abstract

In design studies of Japanese sodium-cooled fast reactors, a compact size reactor vessel is expected to be employed for economical advantages. However, such a design makes coolant velocity higher and may result in occurrence of gas entrainment (GE) phenomena. Since the GE is highly non-linear and too difficult to predict its onset condition by theoretical methods, we are developing a high-precision CFD method to evaluate the GE accurately. The CFD method is formulated on unstructured meshes to establish accurate geometric modeling of complicated reactor systems. As for two-phase flow simulations, a high-precision volume-of-fluid algorithm was employed and newly formulated on unstructured meshes. In the formulation process, a volume-conservative algorithm and a new formulation establishing the mechanical balance between pressure and surface tension were introduced. The developed CFD method was verified by solving well-known driven-cavity and Zalesak's slotted-disk rotation problems to show the simulation accuracy. Then, we simulated a rising bubble in liquid under Bhaga *et al*'s experimental conditions. As a result, the developed method showed good agreement with the experiment. Finally, the developed method was validated by simulating the GE phenomena in the basic experiment. The developed method succeeded in reproducing the occurrence of the GE under the experimental GE condition.

1. INTRODUCTION

Fast breeder reactors (FBRs) are located as one of the possible energy source in the future, with the object of not only effective use of resources but also environmental conservation. In Japan, a sodium-cooled fast reactor (JSFR) was selected as a possible option due to its high competitiveness in power costs (Ichimiya, 2003) and the fast reactor cycle technology development (FaCT) project has been conducted by JAEA and related organizations. As an important part of the FaCT project, more compact reactor vessel have been studied to enhance the economical competitiveness of the JSFR (Kimura, 2005). However, such a design concept may result in occurrence of cover gas entrainment (GE) from free surface because coolant velocity in the primary system becomes larger and the larger coolant velocity can induce free surface fluctuation in upper plenum region of the reactor vessel. Since bubbles entrained to the coolant due to the GE might cause power disturbance when they go through the reactor core, the GE must be prevented from occurring in the JSFR for a stable operation.
The GE phenomena have been studied experimentally and theoretically in many years (Maier, 1998). In those studies, onset conditions of the GE were investigated using experimental systems consisting of reservoir tanks or main pipes with branches (suction pipes). From the experimental results, the correlation of the onset condition was formed as an equation of Froude number (Fr) and branch diameter (Zuber, 1980) and the equation is widely accepted among the researchers. However, some experimental results disagreeing with the equation were reported for the vortical type GE (Daggett, 1974) because effects of Reynolds or Weber numbers become significant in the vortical type GE. Also in GE studies for the FBR systems, experimental results showed that the onset condition of the vortical type GE was dominated by the liquid velocity itself, not the Fr number (Eguchi, 1984). Therefore, it can be expected that the vortical type GE needs special treatment to predict its onset condition. In such cases, full-scale experiments can be a reliable way to evaluate the onset condition

of the GE in each system. However, considering very high costs and difficulties in measurements, full-scale experiments may not be the best way to evaluate the GE. Recently, numerical simulations can be considered to be promising ways as substitutions of the full-scale experiments owing to the progress of computer systems and numerical methods.

In this paper, we develop and validate a high-precision CFD method to evaluate the GE phenomena accurately. The CFD method is formulated on unstructured meshes to establish accurate geometric modeling of complicated reactor systems and to simulate complicated flow pattern accurately in the reactor systems. As a two-phase flow simulation method, a volume-tracking algorithm based on a high-precision volume-of-fluid, namely PLIC (Piecewise Linear Interface Calculation, Young, 1982), is employed and newly formulated on unstructured meshes based on the conventional formulations on structured meshes. The developed CFD method is verified by solving well-known driven-cavity and Zalesak's slotted-disk rotation (Zalesak, 1979) problems to show that our CFD method has comparable or higher simulation accuracy than conventional high-precision methods. We also formulate a new volume-conservative algorithm establishing perfect volume conservation for each phase (gas and liquid phases). In addition, new algorithms were introduced to velocity and pressure calculation procedures of the CFD method. We show that the collocated variable arrangement employed in our CFD method often causes instabilities resulting in unphysical solutions. By careful investigations of the instabilities, we conclude that the unphysical behaviors were induced by inappropriate calculations of momentum and velocity-pressure coupling near gas-liquid interface. Therefore, new mechanistic formulations are introduced to improve the unphysical behaviours. For the momentum equation, each phase's velocities near the interface are defined independently using volume fraction values, instead of being calculated from momentum and density values at each mesh cell (like conventional methods). For the velocity-pressure coupling equation, we focus on a mechanical balance condition between pressure and surface tension and formulate localized pressure gradient calculation procedure. Then, the CFD method is applied to rising bubble problem for the validation of the adequacy on dynamic gas-liquid two-phase flow simulations. The parametric simulations are conducted on Morton numbers and the simulation results of rising bubble shapes are compared to the experimental results. Finally, the CFD method is validated by simulating the GE in Okamoto's basic GE experiment (Okamoto, 2004).

2. FORMULATION OF CFD METHOD

2.1 FLOW CALCULATION ON UNSTRUCTURED MESHES

For numerical simulations on unstructured meshes, the collocated variable arrangement is usually employed (e.g. Barth, 1989). Therefore, we also employed the collocated variable arrangement and defined all variables at centers of mesh cells. Then, the finite-volume discretizations were conducted for basic equations, namely the Navier-Stokes (N-S) and the Poisson equations. In addition, the unsteady, advection and diffusion terms in the N-S equation were discretized by the first order Euler explicit, the second order upwind and the second order center schemes, respectively. It should be noted that the second order center scheme was constructed using the deferred-correction method (Muzafefija, 1994) in our study. The velocity-pressure coupling is achieved by the SMAC algorithm (Amsden, 1970). The second order upwind scheme was formulated as: 1) vertex values are estimated as weighed averages of cell (center) values (shown in Fig. 1(a)); 2) face values are interpolated using vertex values; 3) gradient values at cell centers are evaluated by Gauss-Green theorem (Eq. (1)); and 4) fluxes through faces from upwind cells to downwind cells are calculated using cell values and gradient values (Eq. (2)). In Fig. 1(a), each triangle shows mesh cells and values numbered from ϕ_1 to ϕ_6 show cell values. Vectors numbered from $\vec{r}_{v1}$ to $\vec{r}_{v6}$ are connecting each cell centers and the vertex. Those vectors are used to calculate weights for each cell value when the vertex value is estimated as the weighted average of the cell values. This procedure of the weighted averaging was proposed by Kim *et al* (2003) and is considered to lead more accurate fluxes on faces than conventional simpler procedures. Equations (1) and (2) are written as

$$\left(\nabla\phi\right)_c = \frac{1}{V}\int_{\Sigma}\phi_f d\vec{A} = \frac{1}{V}\sum_f \phi_f \vec{A}, \tag{1}$$

$$\phi_f = \phi_c + (\nabla\phi)_c \cdot \vec{r}_{cf}, \tag{2}$$

where ϕ contains velocity, pressure and volume fraction values. V is a cell volume and $\vec{A}$ is a face vector indicating each face area by its norm and face normal direction. $\vec{r}_{cf}$ is a vector connecting cell and face centers in a upwind cell (shown in Fig. 1(b)). Subscripts *v*, *c* and *f* indicates vertex, cell and face values, respectively. Summation in Eq. (1) is conducted for every faces on a cell.

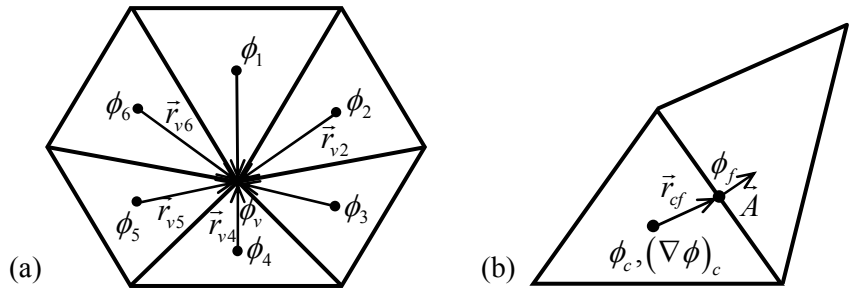

Fig. 1: Schematic View of Second Order Upwind Scheme on Unstructured Mesh: (a) Weighted Averaging to Estimate Vertex Value, (b) Flux Calculation on Mesh Cell Face

2.2 HIGH-PRECISION VOLUME-OF-FLUID METHOD ON UNSTRUCTURED MESHES

For two-phase flow simulations, the transport equation of the volume fraction defined as

$$\frac{\partial f}{\partial t} + \nabla \cdot (\vec{u} f) - f \nabla \cdot \vec{u} = 0, \tag{3}$$

where f is volume fraction which changes from zero to unity and $\vec{u}$ is velocity vector, is solved. The volume fraction indicates mesh cell properties, i.e., mesh cell is filled with liquid if f is unity, filled with gas if f is zero and the interface is located in the cell if f is between zero and unity. In the procedures of the PLIC method: 1) interfacial gradient vectors $\vec{n}$ at each interfacial cell are calculated by the volume fraction distributions around the interfacial cell; 2) interfaces in each interfacial cell are reconstructed utilizing piecewise linear planes; 3) advection fluxes of the volume fraction through each faces are calculated based on locations of reconstructed interfaces; and 4) the volume fraction distributions at next time level are determined.

In our CFD method, the interfacial gradient vector is calculated by the Gauss-Green theorem (shown in Section 2.1) based on given volume fraction distributions. Then, the interface reconstruction is conducted using the calculated interfacial gradient vectors. The interface is reconstructed as the piecewise linear plane normal to the interfacial gradient vector and dividing the interfacial cell into two regions (liquid and gas) that are consistent with the volume fraction of the interfacial cell. In general, the reconstruction is conducted by the Newton-Raphson method (iterative method) (Rider, 1998). However, the direct calculation method (non-iterative method) in which a cubic equation was solved for the reconstruction was developed on the structured mesh and reported to lead more accurate solution with shorter calculation time (Scardvelli, 2000). This direct method was already extended to two-dimensional unstructured meshes to make calculation time shorter also on unstructured meshes (Yang, 2006). We developed a new direct calculation method for three-dimensional unstructured meshes. For calculations of advection fluxes through faces, the multi-dimensional method was employed instead of the conventional operator-splitting method because the multi-dimensional method was reported to lead more accurate solutions than the operator-splitting method (Pilliod, 1998).

In the multi-dimensional advection of the volume fraction, an undershoot (< 0) or overshoot (> 1) of the volume fraction may occur when net outflow quantity of the volume fraction from a mesh cell overcomes the initial volume fraction of the cell (in the case of the undershoot). In general, the undershoot or overshoot is eliminated by clipping the negative value or the value over unity, respectively. However, this clipping procedure changes the total volume of each phase and the volume conservation is not satisfied. In our CFD method, to formulate a physically suitable correction method for the undershoot or overshoot, the additional formulation was introduced to the advection calculation of the volume fraction. Namely, if the undershoot or overshoot of the volume fraction

occurred in a mesh cell after the advection calculation, the advection fluxes through each face are corrected to eliminate the undershoot or overshoot. The volume fraction at new time level is determined using the corrected advection fluxes. In this paper, the correction method for the undershoot is presented but the overshoot can be corrected by similar manner. When the undershoot occurs in a mesh cell, the initial volume fraction in the cell is smaller than the net outflow flux from the cell. This relationship is written as

$$f^* = f^n + Adv\_In - Adv1 - Adv2 < 0, \tag{4}$$

where f^n is the initial volume fraction, f^* is the preliminary volume fraction (negative value), Adv_In is the net inflow flux, $Adv1$ and $Adv2$ are the outflow fluxes through faces 1 and 2, respectively (in the case of two outflow faces). All these values are normalized by the cell volume. Since it is assumed that Adv_In is not changed by the correction method (this assumption will be discussed below), only $Adv1$ and $Adv2$ are corrected to eliminate the undershoot. For that purpose, the advection fluxes are reduced as

$$Adv1 = Adv1 + f^* \, coef1 \big/ \left(coef1 + coef2 \right),$$
$$Adv2 = Adv2 + f^* \, coef2 \big/ \left(coef1 + coef2 \right), \tag{5}$$

where $coef1$ and $coef2$ are positive values and correction coefficients for $Adv1$ and $Adv2$, respectively. The coefficients are calculated by considering dominance of each outflow flux on the net outflow flux. Using this correction method, the right hand side of Eq. (4) becomes zero and the undershoot can be eliminated. However, if Adv_In decreases during the correction of the outflow fluxes, the right hand side of Eq. (4) is still negative after the correction procedure and the correction method must be applied again. Since this repetition increases the computational costs, the inflow flux to the undershoot cell is fixed during the correction procedure.

2.3 PHYSICALLY APPROPRIATE FORMULATION OF MOMENTUM CALCULATION

In general finite-volume methods, each mesh cell is defined as a control volume for calculations. Therefore, intermediate velocities which do not establish the continuity condition are calculated as: 1) using the velocity and density at time level n (v^n and ρ^n, respectively), calculate the momentum at time level n (m^n) (Eq. (6)); 2) calculate the momentum fluxes through each face during one time step (Δt) and summarize the momentum fluxes to obtain the momentum change (δm); 3) adding δm to m^n, calculate the intermediate momentum ($m^{n+\delta}$) (Eq. (7)); 4) dividing m^{n+1} by the at density time level n+1 (ρ^{n+1}), calculate the intermediate velocity ($v^{n+\delta}$) (Eq. (8)). It must be noted that only the advection term is discussed here and the diffusion, pressure and external force terms are neglected for simplification. Equations (6)-(8) are written as

$$m^n = \rho^n v^n, \tag{6}$$
$$m^{n+\delta} = m^n + \delta m, \tag{7}$$
$$v^{n+\delta} = m^{n+\delta} / \rho^{n+1}. \tag{8}$$

Though this procedure is appropriate for single-phase simulations, it can be inappropriate for two-phase simulations when large density ratio exists between two phases. For example, we consider the case when liquid (the velocity and density are v_l and ρ_l, respectively) flows into the mesh cell initially filled with gas (the velocity and density are v_g and ρ_g, respectively). If we assume that inflow liquid volume (Q_{in}) is almost same with outflow gas volume (Q_{out}), the intermediate momentum is calculated as

$$\begin{aligned} m^{n+\delta} &= m^n + \{(\rho_l v_l) Q_{in} - (\rho_g v_g) Q_{out}\} / V \\ &\approx \rho_g v_g (1 - f) + \rho_l v_l f, \end{aligned} \tag{9}$$

where $Q_{in} / V = f$ is used to derive the last equation. In general, since the time step is determined to prevent f from taking large value, we assume that $f << 1$. In addition, we impose $\rho_g << \rho_l$ (here, $\rho_l / \rho_g = 1000$ assuming water and air). Therefore, the intermediate velocity is calculated as

$$\begin{aligned} v^{n+\delta} &= m^{n+\delta} / \rho^{n+1} \\ &= \{\rho_g v_g (1 - f) + 1000 \rho_g v_l f\} / (\rho_g + 999 f \rho_g) \\ &\approx (v_g + 999 v_l f\} / (1 + 999 f) \\ &= \alpha v_g + (1 - \alpha) v_l, \end{aligned} \tag{10}$$

where $\alpha = 1 / (1 + 999 f)$. Equation (10) shows that the intermediate velocity is calculated as the ρ_g weighted average of the gas and liquid velocities. Then, substituting 0.01 as the value of f yields:

$$v^{n+\delta} \approx 0.09\, v_g + 0.91\, v_l. \quad (11)$$

Equation (11) shows that even though the volume fraction (ratio of liquid phase) is only one percent, the intermediate velocity is dominated by the liquid velocity. However, considering that the mesh cell is almost occupied by the gas phase, the intermediate velocity seems invalid as the physical value. In fact, when we employed Eq. (6)-(8) to calculate intermediate velocity, unphysical pressure distribution was generated near bubble interface in numerical simulations of a rising bubble in liquid because the excessive pressure were evaluated by solving the Poisson equation to correct unphysical intermediate velocity (shown in Fig. 2). Though this unphysical behavior appears when interface passes across a face (mesh cell face) as described above, the unphysical pressure distribution disappears with the progress of simulations. Therefore, this behavior is not critical for simulations and seems not to be exposed. However, since transient simulation results including unphysical behaviors are not reliable, the appropriate formulation must be derived to eliminate the unphysical behavior.

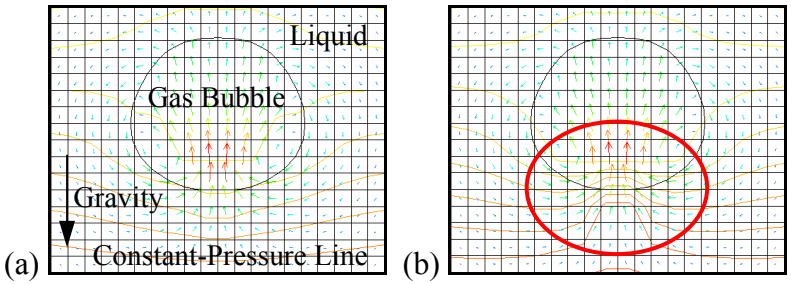

Fig. 2: Unphysical Pressure Distribution Induced by Inappropriate Momentum Calculation

In our CFD method, we improved the momentum calculation procedure. First, the gas and liquid velocities (v_g and v_l, respectively) were independently defined at each interfacial cell. Then, using the gas and liquid velocities, the velocity and the momentum are calculated as : 1) using the velocity, momentum and volume fraction at time level n (v^n, m^n and f^n, respectively), calculate the gas and liquid velocity at time level n (v_g^n and v_l^n, respectively) (Eqs. (12) and (13)); 2) calculate the momentum changes for the gas and liquid phases (δm_g and δm_l, respectively); 3) adding δm_g and δm_l to the gas and liquid momentum at time level n ($m_g^n = \rho_g v_g^n$ and $m_l^n = \rho_l v_l^n$, respectively), calculate the intermediate momentum for the gas and liquid phases ($m_g^{n+\delta}$ and $m_l^{n+\delta}$, respectively) (Eqs. (14) and (15)); 4) divide $m_g^{n+\delta}$ and $m_l^{n+\delta}$ by the gas and liquid densities, respectively, to calculate the intermediate velocity for the gas and liquid phases ($v_g^{n+\delta}$ and $v_l^{n+\delta}$, respectively) (Eqs. (16) and (17)); 5) calculate the intermediate velocity and momentum (Eqs. (18) and (19). Equations (12)-(19) are written as

$$v_g^n = (\rho_l v^n - m^n) / \{(1 - f^n)(\rho_l - \rho_g)\}, \quad (12)$$

$$v_l^n = (m^n - \rho_g v^n) / \{f^n (\rho_l - \rho_g)\}, \quad (13)$$

$$m_g^{n+\delta} = \{(1 - f^n) m_g^n + \delta m_g\} / (1 - f^{n+1}), \quad (14)$$

$$m_l^{n+\delta} = (f^n m_l^n + \delta m_l) / f^{n+1}, \quad (15)$$

$$v_g^{n+\delta} = m_g^{n+\delta} / \rho_g, \quad (16)$$

$$v_l^{n+\delta} = m_l^{n+\delta} / \rho_l, \quad (17)$$

$$v^{n+\delta} = (1 - f^{n+1}) v_g^{n+\delta} + f^{n+1} v_l^{n+\delta}, \quad (18)$$

$$m^{n+\delta} = (1 - f^{n+1}) m_g^{n+\delta} + f^{n+1} m_l^{n+\delta}. \quad (19)$$

These formulations were applied to numerical simulations of a rising bubble in liquid and succeeded in eliminateing the unphysical behavior induced by the conventional method because above formulations can calculate physically appropriate intermediate velocities at each interfacial cell while the intermediate momentum is completely same with the conventional method. In other words, the new formulations can evaluate the intermediate velocity based on the volume fraction without reducing conservation propety of the momentum. It should be noted that though the definition of the new variable at interfacial cells needs additional memory usage, the computational costs do not increase significantly because in general, the ratio of interfacial cells to whole mesh cells is small.

2.4 PHYSICALLY APPROPRIATE FORMULATION OF VELOCITY-PRESSURE COUPLING

The appropriate balance between the pressure and surface tension was already achieved on structured meshes (Francois, 2006). The key to the appropriate balance is formulating the pressure and surface tension in the same form. In other words, the appropriate balance is achieved by defining both the pressure gradient and surface tension on each (mesh cell) face. This appropriate formulation guarantees to eliminate the spurious velocity around spherical bubbles induced by the conventional formulations. However, we can not simply extend the formulations on structured meshes to unstructured meshes because the highly complicated formulation of the pressure gradient than on structured meshes is employed to establish high-precision calculations on unstructured meshes and the complicated formulation prevents the surface tension from being formulated in the same form. In fact, when we employ the deferred-correction method for the pressure gradient calculation, the balance equation between the pressure and surface tension on a face is written as

$$\vec{n}_f \cdot \left\{ \nabla\phi + \frac{\vec{d}_{12}}{\left|\vec{d}_{12}\right|^2}\left(p_2 - p_1 - \vec{d}_{12}\cdot\nabla\phi \right) \right\} = \vec{n}_f \cdot \left(\alpha_1 \vec{F}_1 \, \rho_f^{n+1} / \rho_1^{n+1} + \alpha_2 \vec{F}_2 \, \rho_f^{n+1} / \rho_2^{n+1} \right),$$

$$\nabla\phi = \alpha_1 \left(\nabla p\right)_1 \rho_f^{n+1} / \rho_1^{n+1} + \alpha_2 \left(\nabla p\right)_2 \rho_f^{n+1} / \rho_2^{n+1}, \tag{20}$$

where subscripts 1 and 2 indicate values at mesh cells on both sides of a face. $\vec{n}_f$ is a unit normal vector of a face, $\vec{d}_{12}$ is a vector connecting cell centers from 1 to 2, p is pressure and $\vec{F}$ is surface tension. α_1 and α_2 are weights for interpolating the cell values to a face. In Eq. (20), the pressure gradient (the left hand side) is not written in the consistent form with the surface tension (the right hand side). Therefore, the balance between the pressure and surface tension is not established. Instead of Eq. (20), we derived new formulations in which the appropriate balance is established. First, the right hand side of Eq. (20) was modified to be consistent with the left hand side. Then, Eq. (20) was divided into two equations as

$$\vec{n}_f \cdot \frac{\vec{d}_{12}}{\left|\vec{d}_{12}\right|^2}\left(p_2 - p_1 \right) = \vec{n}_f \cdot \frac{\vec{d}_{12}}{\left|\vec{d}_{12}\right|^2}\left(\varphi_2 - \varphi_1 \right), \tag{21}$$

$$\vec{n}_f \cdot \left\{ \nabla\phi - \frac{\vec{d}_{12}}{\left|\vec{d}_{12}\right|^2}\left(\boldsymbol{d}_{12}\cdot\nabla\phi \right) \right\} = \vec{n}_f \cdot \left\{ \vec{F}_f - \frac{\vec{d}_{12}}{\left|\vec{d}_{12}\right|^2}\left(d_{12}\cdot\vec{F}_f \right) \right\},$$

$$\vec{F}_f = \alpha_1 \vec{F}_1 \, \rho_f^{n+1} / \rho_1^{n+1} + \alpha_2 \vec{F}_2 \, \rho_f^{n+1} / \rho_2^{n+1}, \tag{22}$$

where φ is the surface tension potential calculated by considering the Laplace equation. Our CFD method establishes Eqs. (21) and (22) independently to achieve the appropriate balance between the pressure and surface tension. As for Eq. (21), by introducing suitable surface tension potentials, the pressure values can be uniquely determined at every mesh cells and the appropriate balance between the pressure and surface tension potential is established if the interfacial curvature values are correctly estimated for spherical bubbles. On the other hand, it is much more difficult to establish the balance between the pressure gradient and surface tension in Eq. (22) than to establish Eq. (21) because the formulations of the pressure gradient and surface tension are quite different though the left and right hand sides are written in the same form. While the pressure gradient is calculated by the pressure distribution, the surface tension is defined at each interfacial cell independently. In other words, the number of unknowns in the left hand side of Eq. (22) is k (k is the number of the mesh cell) and is not equal to that in the right hand side ($3k$). Therefore, we modified the formulation of the pressure gradient to be consistent with the surface tension as

$$\nabla p_c = \vec{F}_c + \left(\nabla p\right)_c', \tag{23}$$

where $\left(\nabla p\right)_c'$ is a newly defined variable at each mesh cell and corresponds to a net correction quantity to the intermediate velocity because the velocity at time level $n+1$ is calculated as

$$v^{n+1} = v^{n+\delta} + \left(\nabla p\right)' \Delta t / \rho_c^{n+1}, \tag{24}$$

where the diffusion term and the pressure and external force terms at time level n are considered to calculate the intermediate velocity. By introducing the net correction quantity, the number of unknowns in the left hand side of Eq. (22) reaches to $4k$ and reduced to $3k$ when the pressure values at each mesh cell are determined by Eq. (21). Therefore, the left hand side of the Eq. (22) becomes consistent with the right hand side. In this case, the appropriate balance between the pressure gradient and the surface tension can be established when the net correction quantity is zero, i.e. no acceleration associated with the surface tension works on the intermediate velocity. It should be noted that though the definition of the net correction quantity makes the computational costs higher, the costs do not increase significantly because the net correction quantity is defined only at interfacial regions where the surface tension works.

3. VERIFICATION OF CFD METHOD

3.1 VORTEX GROWTH AND DRIVEN-CAVITY PROBLEMS

To verify the flow calculation method formulated in Section 2.1, we calculated the vortex growth and driven-cavity problems. The vortex growth problem is proposed by Bell *et al* (1979) and calculated by some researchers (e.g. Sussman, 2003). This problem treats inviscid flow in which vortices grow. One can know the accuracy of CFD methods by investigating conservation properties of the kinetic energy in this problem. The numerical simulation is conducted in 1.0 x 1.0 square domain subdivided into 256 x 256 square mesh cells. The periodic boundary conditions are applied to all four boundaries. As the initial condition, x (horizontal) and y (vertical) components of velocity (u and v, respectively) are defined as

$$u = \begin{cases} \tanh(30(y - 1/4)) & for \quad y \le 1/2, \\ \tanh(30(3/4 - y)) & for \quad y > 1/2, \end{cases}$$
$$v = (1/20)\sin(2\pi x). \tag{25}$$

Figure 3(a) shows the vortex growth (vorticity distributions) in the simulation domain. The vortices grow rapidly and high vorticity regions are formed. Figure 3(b) shows the loss of the kinetic energy during the calculation (until $t = 2.0$). The total loss of the kinetic energy is about 0.1 percent at $t = 2.0$ and can be negligible in practical simulations. In addition, the accuracy of our CFD method was investigated by conducting grid convergence tests. As a result, it was confirmed that the CFD method had the second order accuracy.

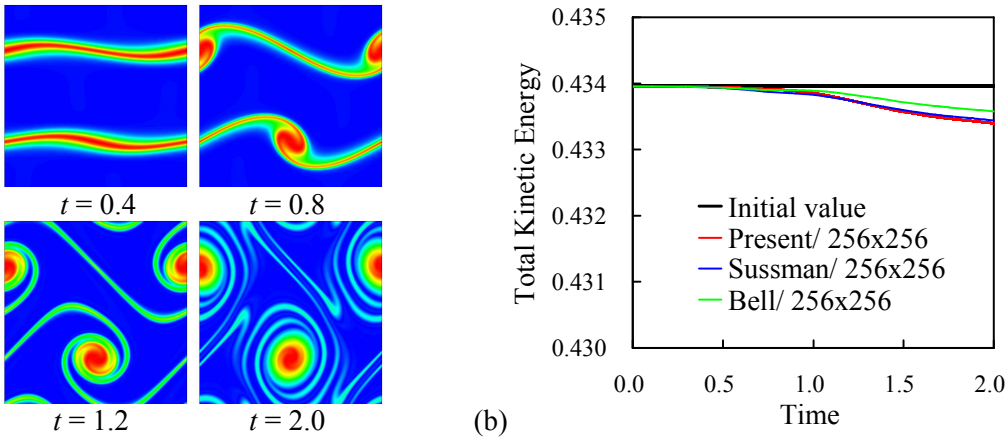

Fig. 3: Simulation Result of Vortex Growth Problem: (a) Vorticity Distribution, (b) Loss of Kinetic Energy

The well-known driven-cavity problem is frequently employed to verify CFD methods. In our study, the cavity is 1.0 x 1.0 square (shown in Fig. 4(a)) and is subdivided into 40 x 40 square mesh cells (structured mesh) or 1,608 triangular mesh cells (unstructured mesh, shown in Fig. 4(b)). The upper

wall is the moving wall with velocity 1.0 and the other walls are non-slip walls. Figure 4(c) shows the velocity distributions on the dashed lines in Fig. 4(a). The result on the structured mesh agrees well with the simulation result in GHIA *et al* (1982). On the other hand, the simulation accuracy somewhat decreases on the unstructured mesh. However, the discrepancy between the results on the structured and unstructured meshes is small enough to conclude that the high-precision simulation is also possible on unstructured meshes.

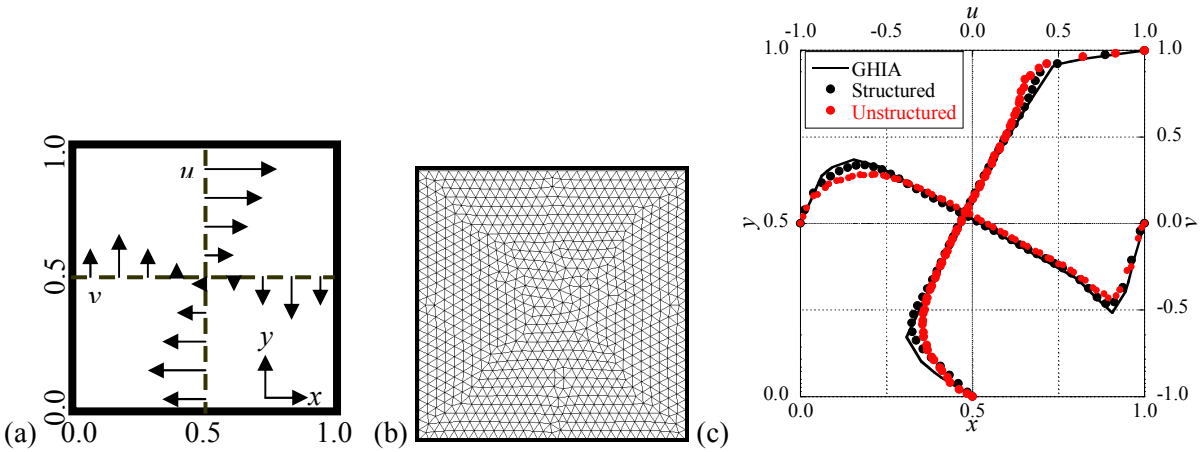

Fig. 4: Simulation Results of Driven-Cavity Problem (Reynolds Number is 1000): (a) Simulation Domain, (b) Unstructured Mesh, (c) Velocity Distribution

3.2 ZALESAK'S SLOTTED-DISK ROTATION PROBLEM

The slotted-disk rotation problem is well-known and frequently used to verify two-phase simulation methods (volume-tracking algorithms). The problem was well summarized in Rudman (1997) and therefore the same simulation conditions were utilized in our study. The simulation domain is 4.0 x 4.0 square in which a circular disk with a radius of 0.5 having a slot with a width of 0.12 is located at (2.0, 2.65). Initially, the volume fraction is set unity in the slotted-disk and zero outside the disk. The slotted-disk is rotated once around the domain center (2.0, 2.0) in the counter-clockwise direction and then the simulation error was estimated as the averaged value of the volume fraction differences at every mesh cells between the initial and the final (after the rotation) states. Number of time marching for one rotation is also the same number (2524 steps) with the Rudman's simulation condition. The structured and unstructured meshes consist of 200 x 200 square mesh cells and 39,734 triangular mesh cells, respectively. Table 1 shows the simulation errors. It is evident that the present method is superior to the conventional volume-tracking algorithms, i.e. SLIC (Simple Line Interface Calculation, Noh, 1976), SOLA-VOF (Hirt, 1981) and FCT-VOF (Rudman, 1997) and is comparable with the high-precision volume-tracking algorithms, i.e. PLIC or Stream (Harvie, 2000) on the structured mesh. Though the simulation error becomes larger on the unstructured mesh, applying the volume conservative algorithm proposed in Section 2.2 highly reduces the simulation error. Therefore, the simulation accuracy of the high-precision volume-tracking algorithm employed in our CFD method was confirmed to be high enough on both structured and unstructured meshes.

Table 1: Simulation Error in Slotted-Disk Rotation Problem

Algorithm	Mesh	Error
SLIC	Structured	8.38×10^{-2}
SOLA-VOF	Structured	9.62×10^{-2}
FCT-VOF	Structured	3.29×10^{-2}
PLIC	Structured	1.09×10^{-2}
Stream	Structured	1.07×10^{-2}
Present (Non-Conservative)	Structured	1.07×10^{-2}
	Unstructured	1.50×10^{-2}
Present (Conservative)	Structured	1.08×10^{-2}
	Unstructured	1.23×10^{-2}

3.3 EVATUATION OF SPURIOUS VELOCITY

To verify the appropriate balance formulation between the pressure and surface tension proposed in Section 2.4, two dimensional numerical simulations of a circular gas bubble in stationary liquid without the gravitational force were conducted. The simulation domain is 40 x 40 square and subdivided into 40 x 40 mesh cells (structured mesh) and 1608 triangular mesh cells (unstructured mesh). The circular gas bubble with a radius of 30.0 is located at the center of the simulation domain. The numerical simulations were assumed to be conducted for the air and water at the room temperature as ρ_g = 1.2929, ρ_l = 998 and σ = 0.0735. The initial velocity and pressure distributions were assumed to be zero in all locations. To the four walls containing the simulation domain, free-slip boundary conditions were applied. The numerical simulations were conducted only for 1 time step (Δt = 10^{-3}), and then we investigated the spurious velocity in the simulation domain. First, we used a correct interfacial curvature value in both numerical simulations by the conventional method and the present method (with the appropriate balance formulation). Then, the similar comparison was conducted in the case when the interfacial curvature values are estimated numerically using the volume fraction distributions. In our CFD method, the interfacial curvature values are numerically estimated by the RDF (Reconstructed Distance Function) model proposed by Cummins *et al* (2005).
The maximum spurious velocities in each simulation result are shown in Table 2. It is well-known that the conventional method generates the spurious velocity even though the correct curvature value is employed in the simulations due to the unbalance formulation between the pressure and surface tension. On the other hand, the present method succeeded in reducing the spurious velocity to machine zero on both the structured and unstructured meshes in the case when the correct curvature value is available. Therefore, in this case, it is evident that the results by the present method experience no unphysical behaviors even if the time step proceeds. When the RDF model was employed to estimate the curvature value, even the present method generated the spurious velocity. However, the norms of the spurious velocities are highly small compared to the conventional method. Therefore, the appropriate balance formulation was confirmed to be efficient for the numerical simulation of two-phase flows. It is very interesting that even when the RDF model was employed, the conventional method gave almost the same results with the results base on the correct curvature value (this tendency was checked by comparing the spurious velocity distributions around the bubble). This fact indicates that the origins of the numerical errors generated in the conventional method are mainly on the unbalance formulation between the pressure and the surface tension. Namely, the numerical errors generated in the estimation procedure of the interfacial curvature values by the modified RDF model are sufficiently small compared to the numerical errors induced by the unbalance formulation. Therefore, we can conclude that unbalance formulations between the pressure and the surface tension should be primarily eliminated to employ the physically appropriate formulation.

Table 2: Maximum Norm for Spurious Velocity

Simulation Methods	Curvature Estimation	Simulation Mesh	Maximum Norm for Spurious Velocity
Conventional	Correct	Structured	8.03×10^{-7}
		Unstructured	3.97×10^{-6}
	RDF	Structured	8.03×10^{-7}
		Unstructured	4.05×10^{-6}
Present	Correct	Structured	2.51×10^{-17}
		Unstructured	5.46×10^{-18}
	RDF	Structured	1.36×10^{-9}
		Unstructured	6.58×10^{-10}

4. APPLICATION TO RISING BUBBLE PROBLEM

For the basic validation of our CFD method, transient behaviors of a rising gas bubble in liquid were numerically simulated and the simulation results were compared to the experimental data. It is well known that transient behaviors of rising gas bubbles in liquid are categorized by the Morton number (M) and the Eotvos number (Eo). For example, a number of experiments with different couplings of

the Morton and the Eotvos numbers were conducted by Bhaga *et al* (1981). In our study, the numerical simulations were conducted for the rising gas bubble in the liquid under Bhaga's experimental conditions of gas and liquid properties. The simulation was conducted on the rectangular region with a height and width of 160 mm and 80 mm, respectively. This region is subdivided into 80 x 40 mesh cells (structured mesh) and 3,234 triangular mesh cells (unstructured mesh, shown in Fig. 5(a)). The center of the circular air bubble with a radius of 26.1 mm is initially located at a height of 30 mm from the bottom of the region. The initial velocity and pressure distributions are zero in all locations. We investigated numerically the transient behaviors of the air bubble for 0.3 second.

The comparisons of the terminal bubble shapes between the simulation and experiment are shown in Fig. 5(b). Under both Morton number conditions, the simulation results agree well with the experimental results even in the cases when the unstructured mesh is employed. Therefore, it was confirmed that the numerical simulations by our CFD method could give physically appropriate solutions for a rising bubble in liquid on both the structured and unstructured meshes.

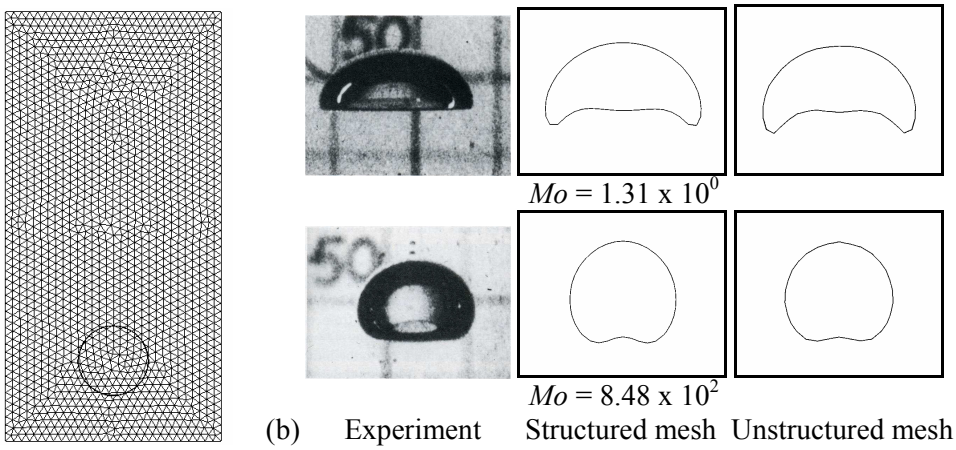

Fig. 5: Simulation Results of Rising Bubble in Liquid: (a) Unstructured Mesh, (b) Comparison of Terminal Bubble Shape (The experimental results are shown in Bhaga *et al* (1981).)

5. NUMERICAL SIMULATION OF GE PHENOMENA

Finally, we applied our CFD method to the GE phenomena in the basic GE experiment. The basic GE experiment consists of a square rod and a suction tube (square tube with an inner edge length of 10mm and a wall thickness of 5.0mm) in a rectangular channel (Okamoto, 2003). Working fluids are water and air. The width of the channel, the initial free surface height from the bottom surface and the edge length of the square rod are 0.20 m, 0.15 m and 0.05 m, respectively. The suction tube is located at 0.05 m downstream of the square rod. The water depth from the free surface to the suction mouth is 0.05 m. In the rectangular channel, inlet flow generates a wake behind the square rod when the flow goes through the square rod. In the wake, vortices are generated and advected downstream. When a vortex flows across the region near the suction tube, the vortex interacts with suction (downward) flow. The vortex core is connected to the suction mouth to be extended by the suction flow and the vortex strength rapidly grows up by the interaction between the vortex and the suction flow. Accompanied by the vortex growth, a gas core is generated on the free surface and the stronger the vortex grows, the deeper the gas core develops. Finally, when the gas core highly develops and reached to the mouth of the suction tube, the gas is entrained into the suction tube (occurrence of the GE). Figure 6(a) shows the simulation mesh in which all mesh cells are hexahedral. Since the GE occurs in the region near the suction tube, a finer mesh subdivision applied to the region is necessary for the accurate numerical simulations. Therefore, the mesh cell size in the region near the suction tube is about 2.0 mm, around the rod region is 3.0 mm and the other regions is 6.0 mm. As for the vertical mesh subdivision, to simulate the free surface deformation closely, the region near the free surface level is subdivided into about 2.0 mm. The simulation was conducted under the GE condition, i.e. the condition under which the GE was observed in the experiment. In this condition, the inlet velocity is 0.10 m/s and the suction velocity is 4.0 m/s. In addition, the static pressure condition was applied to the outlet in the simulation.

Figures 6(b) and 6(c) show the simulation results for the free surface shape (the occurrence of the GE) and the transient vortical velocity distributions above the suction tube, respectively. As shown in Fig. 6(b), our CFD method succeeded in reproducing the GE occurrence observed in the experiment under the same condition. In addition, it was confirmed that the GE in the simulation result was induced by the same mechanism with the experiment. In other words, as mentioned above, the interaction between the vortex (free surface) and the suction flow induces the GE in the experiment, in the simulation result (shown in Fig. 6(c)), it is evident that the growth of the suction velocity towards the free surface extends the gas core and causes the GE. Therefore, form these simulation results, our CFD method was validated to be applicable to the GE phenomena.

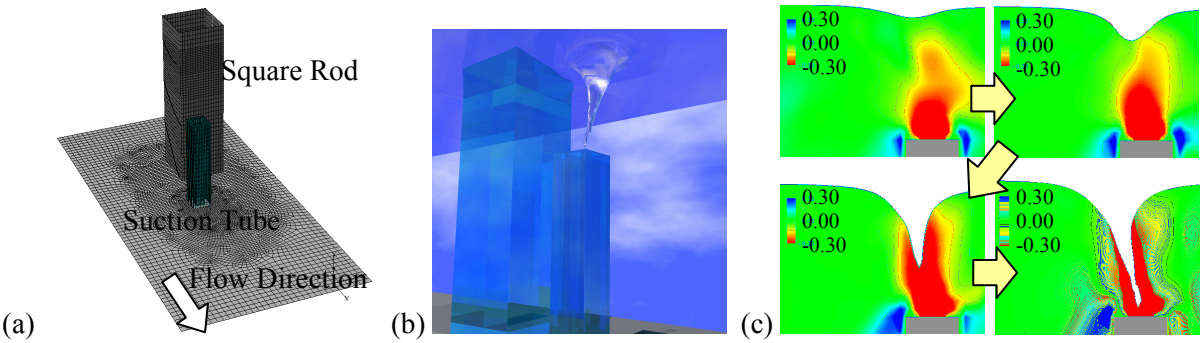

Fig. 6: Simulation Result of GE: (a) Simulation Mesh, (b) Occurrence of GE, (c) Transient Vertical Velocity Distribution (m/s)

6. CONCLUSION

In this paper, we developed and validated a high-precision CFD method to evaluate the GE phenomena accurately. First, the flow calculation method on unstructured meshes were formulated and verified. As a result, our CFD method succeeded in calculating vortical flows accurately even on the unstructured mesh. Second, the PLIC method was newly formulated on unstructured meshes and verified by solving the slotted-disk rotation problem. In addition, the volume-conservative formulation was introduced to improve the simulation accuracy on unstructured meshes. Third, the appropriate momentum calculation method and the appropriate balance between the pressure and surface tension were addressed to eliminate the unphysical behaviors (e.g. spurious velocity) generated in conventional methods. Our new formulation succeeded in eliminating the unphysical behaviors near gas-liquid interface and deriving physically appropriate solutions. Finally, the CFD method was applied to the rising bubble problem and the GE phenomena. As a result, the simulation results of the rising bubble in liquid agreed well with the experimental data. In addition, the occurrence of the GE in the basic GE experiment was reproduced by the simulation. These validation results show that our CFD method is confirmed to be applicable to the numerical simulation of the GE phenomena.

REFERENCES

A. A. Amsden, F. H. Harlow, "The SMAC method: a numerical technique for calculating incompressible fluid flows", Technical Report LA-4370, Los Alamos National Laboratory, (1970).

T. J. Barth, D. C. Jespersen, "The Design and Application of Upwind Schemes on Unstructured Meshes", *27th Aerospace Sciences Meeting*, AIAA-89-0366, (1989).

J. B. Bell, P. Colella, H. M. Glaz, "A second order Projection Method for the incompressible Navier-Stokes Equations", J. Comput. Phys. 85 (1989) 257-283

D. Bhaga, M. E. Weber, "Bubbles in viscous liquid: shapes, wakes and velocities", *J. Fluid. Mech.*, 105, 61-85 (1981).

S. Cummins, M. M. Francois, D. B. Kothe, "Estimating curvature from volume fractions", *Computer & Structure*, 83 425-434 (2005).

L. L. Daggett, G. H. Keulegan, “Similitude in Free-Surface Vortex Formations”, *Journal of the Hydraulics Division*, *Proceedings of the ASCE*, Vol. 100, No. HY8 (1974).

Y. Eguchi, K. Yamamoto, T. Funada, N. Tanaka, S. Moriya, K. Tanimoto, K. Ogura, K. Suzuki, I. Maekawa, “Gas Entrainment in the IHX of Top-Entry Loop-Type LMFBR”. *Nucl. Eng. Des.*, 146, 373-381 (1984).

M. M. Francois, S. J. Cummins, E. D. Dendy, D. B. Kothe, J. M. Sjicilian, M. W. Williams, “A balanced force algorithm for continuous and sharp interfacial surface tension models within a volume tracking framework”, *J. Comput. Phys.*, 213, 141-173 (2006).

U. GHIA, K. N. GHIA, C. T. SHIN, “High-Re Solutions for Incompressible Flow Using the Navier-Stokes Equations and a Multigrid Method”, *J. Comput. Phys.*, 48, 387-411 (1982).

D. J. E. Harvie, D. F. Fletcher, “A New Volume of Fluid Advection Algorithm: The Stream Scheme”, *J. Comp. Phys.*, 162, 1-32 (2000).

C. W. Hirt, D. B. Nichols, “Volume of Fluid (VOF) Method for the Dynamics of Free Boundaries”, *J. Comp. Phys.*, 39, 201-205 (1981).

M. Ichimiya, T. Mizuno, M. Konomura, “A Promising Sodium-Cooled Fast Reactor Comcept and its R&D Plan”, *GLOBAL 2003*, New Orlens, LA, USA (2003).

S. E. Kim, B. Makarov, D. Caraeni, “A Multi-Dimensional Linear Reconstruction Scheme for Arbitrary Unstructured Grids”, AIAA 2003-3990 (2003).

N. Kimura, K. Hayashi, M. Igarashi, H. Kamide, M. Itoh, T. Sekine, “Experimental study on flow optimization in upper plenum of reactor vessel for a compact sodium cooled fast reactor”, *Nucl. Tech.*, 152, 210-222 (2005).

M. R. Maier, “Onsets of liquid and gas entrainment during discharge from a stratified air-water region through two horizontal side branches with centerlines falling in an inclined plane”, M. Sc. Thesis, University of Manitoba (1998).

P. A. Muzaferija, “Adaptive finite volume method for flow predictions using unstructured meshes and multigrid approadh”, Ph.D. thesis, Univ. of London (1994).

W. F. Noh, P. Woodward, “SLIC (Simple Line Interface Calculation)”, *Lecture Notes in Physics*, (A. I. van der Vooren, P. J. Zandbergen, ed.), Springer-Verlag, 330-340 (1976).

K. Okamoto, K. Takeyama, M. Iida, “Dynamic PIV Measurement for the Transient Behavior of a Free-Surface Vortex”, *Forth Japan-Korea Symposium on Nuclear Thermal Hydraulics and Safety* (NTHAS4), Sapporo, Japan, NTHAS4-097 (2004).

J. E. Pilliod, E. G. Puckett, “Second-Order Accurate Volume-of-Fluid Algorithms for Tracking Material Interfaces”, *J. Comp. Phys.*, 199, 465-502 (2004).

W. Rider, D. B. Kothe, “Reconstructing Volume Tracking”, *J. Comp. Phys.*, 141,112-152 (1998).

M. Rudman, “Volume-Tracking Methods for Interfacial Flow Calculations”, *Int. J. Numer. Methods Fluids*, 24, 671-691 (1997).

R. Scardvelli, S. Zaleski, “Analytical Relations Connecting Linear Interface and Volume Functions in Rectangular Grids”, *J. Comp. Phys.*, 164, 228-237 (2000).

M. Sussman, “A second order coupled level set and volume-of-fluid method for computing growth and collapse of vapor bubbles”, *J. Comput. Phys.*, 187, 110-136 (2003).

X. Yang, A. J. James, “Analytic Relations for Reconstructing Piecewise Linear Interfaces in Triangular and Tetrahedral Grids”, *J. Comp. Phys.*, 214, 41-54 (2006).

D. L. Young, (K. W. Morton, M. J. Baine, ed.), *Numerical Methods for Fluid Dynamics*. Academic Press, 273-468 (1982).

S. T. Zalesak, “Fully Multidimensional Flux-Corrected Transport Algorithm for Fluids”, *J. Comp. Phys.*, 31, 335-362 (1979).

N. Zuber, “Problems in Mod eling of Small Break LOCA”, *Nuclear Regulatory Commission Report*, NUREG-0724 (1980).